A quantum mechanical investigation of the electronic and magnetic properties of $CaMnO_3$ perovskite



1997 J. Phys.: Condens. Matter 9 489

(http://iopscience.iop.org/0953-8984/9/2/016)

J. Phys.: Condens. Matter **9** (1997) 489–498. Printed in the UK PII: S0953-8984(97)76780-8

# A quantum mechanical investigation of the electronic and magnetic properties of $CaMnO_3$ perovskite

F Freyria Fava†, Ph D'Arco‡, R Orlando† and R Dovesi†

† Department of Inorganic, Physical and Materials Chemistry, University of Torino, via P Giuria 5, I-10125 Torino Italy

‡ Laboratoire de Géologie, Ecole Normale Supérieure, 24 rue Lhomond, 75005 Paris, France

Received 31 July 1996

**Abstract.** The ground-state electronic structures of ferromagnetic and antiferromagnetic $CaMnO_3$ perovskite in the ideal cubic phase have been investigated using the *ab initio* periodic Hartree–Fock approach. The system is a wide-gap insulator. The antiferromagnetic phase is correctly predicted to be the more stable (0.07 eV per Mn atom at the equilibrium geometry), but the superexchange interaction is substantially overestimated. The energy difference between the two phases increases slowly and linearly under compression, at variance with that for $KMF_3$ (M = Ni, Mn), that shows an exponential behaviour when the M–M distance is reduced. As regards the electronic structure, three unpaired electrons occupy very localized $t_{2g}$-type d orbitals on Mn. About 1.8 electrons (according to a Mulliken partition scheme for the electronic charge) occupy Mn $e_g$-type states ($d_{z^2}$ and $d_{x^2-y^2}$ Mn d orbitals), which however overlap significantly with oxygen p orbitals; the degree of spin polarization of these bond states is very low. The electronic structure of the system is discussed in terms of the density of states and charge- and spin-density maps.

## 1. Introduction

Perovskite structure is an important structural type adopted by numerous compounds with $ABX_3$ stoichiometry, where A and B are cations and X represents anions such as those of oxygen or fluorine. These materials have been extensively studied because of their magnetic [1–4] and ferroelectric [5] properties. Among these compounds $CaMnO_3$ perovskite plays a special rôle because it is the archetype of perovskite-related compounds such as $Ca_2MnO_4$ and $CaMnO_{2.5}$ [6]. The latter is a crystalline compound with ordered oxygen vacancies obtained by reduction of $CaMnO_3$ at low temperature [6, 7]. $CaMnO_3$ and related materials such as $Ca_2MnO_4$, $Ca_3Mn_2O_7$, and $Ca_4Mn_3O_{10}$ were investigated in the first study of restricted-dimension magnetic materials [8].

In this paper we investigate with an *ab initio* quantum mechanical tool the electronic and magnetic properties of $CaMnO_3$ perovskite. To our knowledge, this is the first study of this kind on these materials. $CaMnO_3$ is known to be orthorhombic [6] with nearly perfect octahedra rotated by about 8° with respect to the ***b***- and ***c***-axes. As the orthorhombic unit cell contains 20 atoms, the calculation is too expensive at the moment; in this study the ideal cubic structure (5 atoms/cell), consisting of an infinite array of untilted octahedra, has thus been investigated. The present method, in its unrestricted Hartree–Fock version [9] which allows the investigation of open-shell structures, has been applied in previous studies to simple transition metal oxides (MnO, NiO [10, 11]), complex oxides ($Fe_2O_3$ [12]), perovskites ($KMnF_3$, $KNiF_3$ [3]), layered perovskites ($K_2MnF_4$, $K_2NiF_4$ [4]) and Jahn–Teller-distorted perovskites ($KCuF_3$ [13]).

0953-8984/97/020489+10$19.50  

## 2. Computational details

The implementation of the *ab initio* self-consistent-field (SCF) Hartree–Fock LCAO computational scheme for periodic systems within the CRYSTAL code [14] has been described in previous papers [15, 16]. Values of 7, 7, 7, 7 and 14 have been used for the parameters controlling the direct-space summations for the Coulomb and exchange series (see [14–16] for more details); the reciprocal-space integration was performed by sampling the Brillouin zone in a regular mesh of points defined by a shrinking factor, IS, of 8 (29 asymmetric $k$-points); the energy difference with respect to a calculation performed with IS = 12 is less than $10^{-7}$ Hartree/cell.

Extended Gaussian basis sets composed of 27, 22 and 13 'atomic orbitals' (AOs) have been used for Mn, Ca and O, respectively, where each orbital is a linear combination (contraction) of Gaussian-type functions. The Mn and O basis sets are the same as those used in the MnO study [10], the only difference being that the exponent of the most diffuse d shell of Mn and sp shell of O ($\alpha_{Mn} = 0.259$ Bohr$^{-2}$ instead of 0.249 Bohr$^{-2}$; $\alpha_O = 0.19$ Bohr$^{-2}$ instead of 0.180 Bohr$^{-2}$) and the scale factor of the 4G–d contraction in Mn (1.02 instead of 1.00) have been reoptimized. For Ca, the basis set is the same as in a previous study of $CaF_2$ [17].

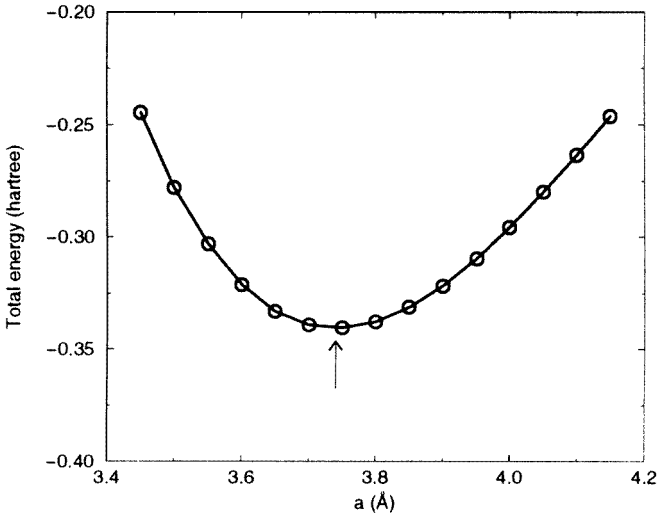


**Figure 1.** The total energy of antiferromagnetic $CaMnO_3$ as a function of the lattice parameter. Symbols and the arrow indicate the calculated energy points and the equilibrium lattice parameter respectively.

## 3. Results and discussion

### *3.1. The structural data*

The total energy of the system as a function of the lattice parameter for the antiferromagnetic (AFM) phase is shown in figure 1. The calculated equilibrium lattice parameter is 3.75 Å, and the bulk modulus (evaluated by interpolation from the energy points of

figure 1 using polynomials of various degrees) is 215 GPa. The binding energy is 0.44 Hartree (275 kcal $mol^{-1}$) per formula unit, resulting from the difference between the bulk total energy ($E = -2051.3401$ Hartree) and the total energy of the isolated atoms ($E_{Ca} = -676.7258$, $E_{Mn} = -1149.7916$, $E_O = -74.7943$). The atomic total energies have been obtained with the basis sets used for the bulk, to which one (Mn) and two (Ca) diffuse Gaussian functions have been added in order to better describe the valence wavefunctions (see references [10, 17] for details for the cations). The experimental study by Poeppelmeier *et al* [6] shows that $MnO_6$ octahedra in orthorhombic $CaMnO_3$ are almost perfectly regular; the mean MnO distance is 1.899 Å, with a standard deviation of 0.004 Å, corresponding to a hypothetical pseudocubic lattice parameter of 3.80 Å, to be compared with 3.75 Å as calculated with the present method. The small underestimation of the Mn–O distance is to be attributed to the compression of the bond in the cubic structure which is necessary to compensate the strong O–O short-range repulsion; a similar effect was observed in the study of cubic $MgSiO_3$ perovskite [18]; when $MgSiO_3$ was allowed to relax to a tetragonal or orthorhombic geometry a much better agreement with experiment was observed for the Si–O distance. To the authors' knowledge, the binding energy and the bulk modulus of the present system have not been determined experimentally.

**Table 1.** Mulliken population data for the ferromagnetic (FM) and antiferromagnetic (AFM) solutions: $Q$, $q$(3d) and $q$(4sp) are the net atomic charge and the populations of the 3d and 4sp orbitals (in electrons) respectively; $N_s$, $n_s$(3d) and $n_s$(4sp) are the corresponding spin quantities. O–X is the bond population between oxygen and its first neighbours of type X. The bond population between Ca and Mn is zero.

| | Mn | | Ca | | O | |
|---|---|---|---|---|---|---|
| | FM | AFM | FM | AFM | FM | AFM |
| $Q$ | +2.16 | +2.17 | +1.86 | +1.86 | −1.34 | −1.34 |
| $q$(3d) | 4.68 | 4.67 | 0.09 | 0.09 | — | — |
| $q$(4sp) | 0.16 | 0.19 | 0.05 | 0.05 | — | — |
| $N_s$ | 3.17 | 3.25 | 0.00 | 0.00 | −0.06 | 0.00 |
| $n_s$(3d) | 3.16 | 3.22 | 0.00 | 0.00 | — | — |
| $n_s$(4sp) | 0.01 | 0.03 | 0.00 | 0.00 | — | — |
| O–X | 0.07 | 0.07 | 0.00 | 0.00 | −0.01 | −0.01 |

### *3.2. The electronic structure*

The electronic structure of $CaMnO_3$ can be analysed with the help of the projected density of states (PDOS), shown in figure 2, and of the Mulliken charge distribution, reported in table 1. The PDOS of the AFM phase (more stable than the FM phase) is shown in figure 2 at the top. The contributions from $t_{2g}$ d and $e_g$ d electrons to the total DOS and from oxygen s and p valence electrons are reported. As the contribution from Ca is completely absent and that from Mn 4sp orbitals is very small (the Mn 4sp shell contains only 0.2 of an electron, as shown in table 1), all of the relevant contributions to the valence and lowest conduction states are actually shown in the figure. Zero energy corresponds to the Fermi level, so occupied and empty states are characterized by negative and positive energies, respectively. As a last comment, it should be noted that both Mn and O projections refer to a single-atom contribution (oxygen contributions are to be multiplied by 3 in order to

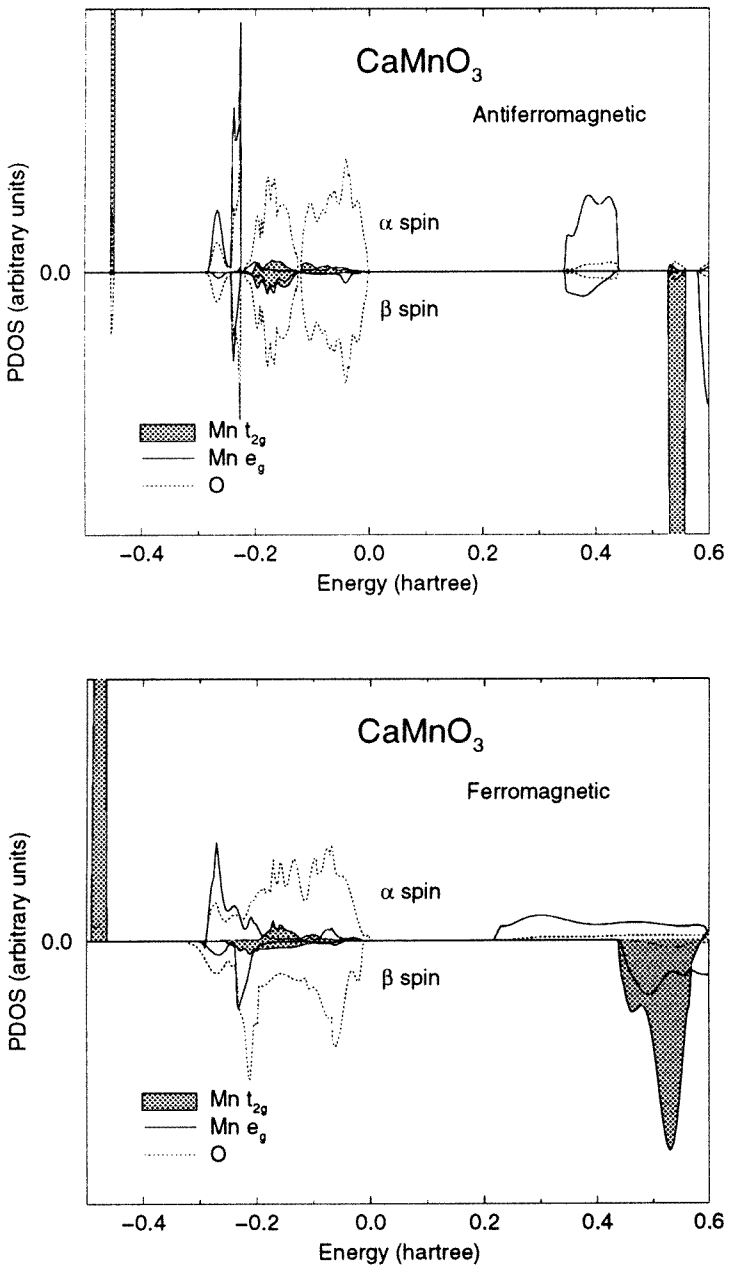


**Figure 2.** Projected densities of states for the valence (negative energies) and conduction (positive energies) bands in the antiferromagnetic (top) and ferromagnetic (bottom) phases.

obtain the stoichiometric ratio 1:3 with Mn and Ca). The figure shows that $CaMnO_3$ is a large-gap (8.9 eV) insulator, and the highest occupied and the lowest unoccupied orbitals can be identified as oxygen p and (nearly pure) manganese $e_g$ atomic orbitals. The present compound can thus be classified as a charge-transfer (O to Mn) insulator.

**Table 2.** Mulliken population data for the FM and AFM solutions: $q$ is the population (in electrons) of the d (Mn) or p (O) orbitals; $n_s$ is the corresponding spin quantity. The Mn and O atoms are along the $x$-axis. The headings 'Inner' and 'Outer' refer to the most contracted and diffuse of the two d (Mn) and p (O) valence shells.

| | | Mn | | | | | O | | | |
|---|---|---|---|---|---|---|---|---|---|---|
| | | FM | | AFM | | | FM | | AFM | |
| | 3d | Inner | Outer | Inner | Outer | 2p | Inner | Outer | Inner | Outer |
| $q$ | $t_{2g}$ | 0.97 | 0.13 | 0.97 | 0.13 | $p_x$ | 1.23 | 0.37 | 1.23 | 0.37 |
| | $e_g$ | 0.37 | 0.33 | 0.37 | 0.33 | $p_{y,z}$ | 1.41 | 0.51 | 1.41 | 0.51 |
| $n_s$ | $t_{2g}$ | 0.91 | 0.03 | 0.91 | 0.02 | $p_x$ | −0.13 | 0.01 | 0.00 | 0.00 |
| | $e_g$ | 0.15 | 0.02 | 0.16 | 0.05 | $p_{y,z}$ | 0.03 | 0.00 | 0.00 | 0.00 |

The valence bands are characterized by a sharp (nearly atomic) pure Mn $t_{2g}$ d peak at −0.45 Hartree (−12.25 eV); the oxygen contribution to this peak, which contains $\simeq 3$ $\alpha$-spin electrons, is negligible, and the $\beta$-spin components are negligible, too. This narrow $t_{2g}$ peak is very localized on the Mn atom, with minor overlap terms with oxygen neighbours, and is separated from the upper valence band by a large gap (0.17 Hartree = 4.5 eV); the Mn $e_g$ contribution to the latter is mainly concentrated at the bottom, whereas the top of the band is dominated by oxygen contributions. Note, however, that there is a high contribution from oxygen to the states in the lower-energy range of the upper valence band, whereas $t_{2g}$ and $e_g$ contributions to the top of the band are negligible. The other important feature to be noticed is that in this upper valence band the $\alpha$- and $\beta$-spin peaks of Mn and O are very similar and do not contribute appreciably to the spin polarization of the cell. This interpretation is confirmed by the data reported in table 1; the Mulliken net charges are +2.17, +1.86 and −1.34 for Mn, Ca and O respectively, quite far from the formal ionic charges $Mn^{4+}$, $Ca^{2+}$ and $O^{2-}$; the reason for this is that, although $CaMnO_3$ is still fairly ionic, there is a large overlap between the Mn $e_g$ d and oxygen p orbitals, resulting in a partially covalent character of the bond, as confirmed by the Mn–O bond population (+0.07 $|e|$; note that the bond population tends to be negative between first neighbours in fully ionic compounds, because electron clouds of ions in contact contract as a consequence of Pauli repulsion). The evidence that the $t_{2g}$ distribution is more contracted than that of $e_g$ is given by the populations of the Mn d shells in table 2: whereas 0.13 $|e|$ and 0.97 $|e|$ are found in the more and less diffuse $t_{2g}$ d shells, respectively, about 50% of the population is in the external shell for $e_g$. The bond population is zero (no repulsion between the two ions) for Ca–O and nearly zero for O–O (−0.01 $|e|$). The oxygen–oxygen repulsion is much smaller than that in $MgSiO_3$ [18], where it is the driving force for the rotation of the octahedra (the corresponding bond population can be as large as −0.07 $|e|$). If we now look at the spin quantities, it turns out that the number of unpaired electrons on Mn is very close to three (3.25 $|e|$; $d^3$ configuration), and they are concentrated in the d shell; table 2 (see the $n_s$-rows) shows that the main contribution comes from the $t_{2g}$ orbitals (0.93 of an unpaired electron each), whereas there is only 0.21 of an unpaired electron in each $e_g$ orbital. No net spin polarization is due to Ca and O in the AFM phase. It is interesting to note that the oxygen p orbital along the bond, $p_x$, is much less populated than $p_y$ and $p_z$ (1.60 $|e|$ and 1.90 $|e|$, respectively).

Charge- and spin-density maps are useful complementary tools for the understanding of the electronic structure of the system.

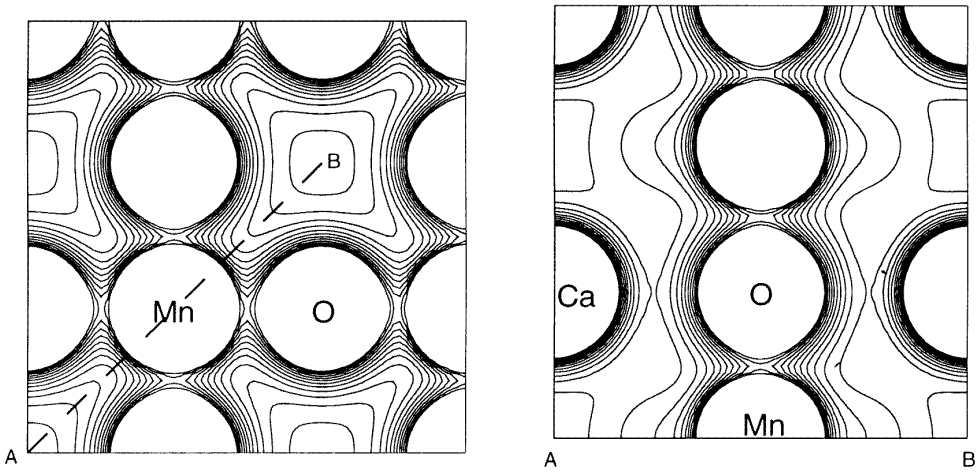


**Figure 3.** Total charge-density maps in the (001) (left) and (110) (right) planes through the atom centres. The dashed line A–B on the left is the trace of the right-hand section. The separation between contiguous isodensity lines is 0.01 $e$ Bohr$^{-3}$. The function is truncated in the core region at 0.12 $e$ Bohr$^{-3}$.

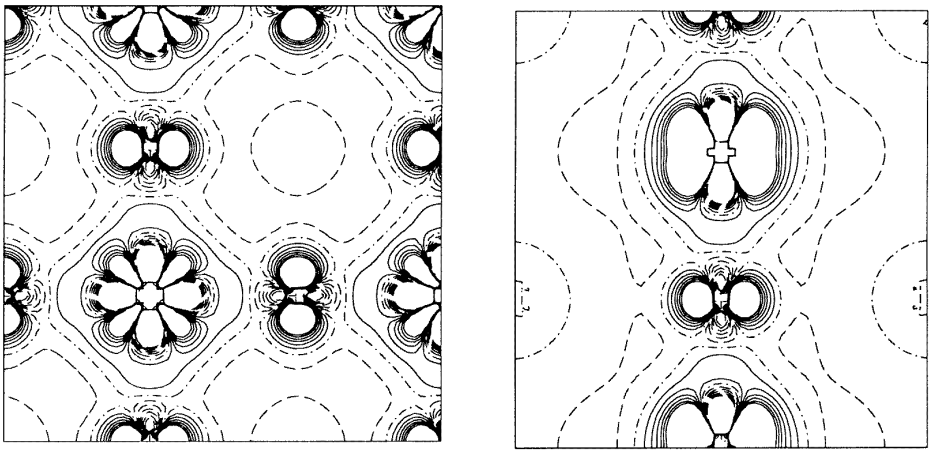

**Figure 4.** Charge-density difference maps showing the difference between the bulk density and the density obtained as the superposition of the densities of isolated (spherical) $Mn^{4+}$, $Ca^{2+}$ and $O^{2-}$ ions. The ionic solutions have been obtained with the same basis as was used for the periodic calculations. The separation between contiguous isodensity lines is 0.005 $e$ Bohr$^{-3}$. The function is truncated in the core region at $\pm 0.03$ $e$ Bohr$^{-3}$. Continuous, dashed and dot-dashed lines correspond to positive, negative and zero values, respectively. The sections are as in figure 3.

In figure 4 the difference between the crystalline total charge density (figure 3) and the superposition of the charge densities of the isolated (spherical) ions ($Ca^{2+}$, $Mn^{4+}$ and $O^{2-}$) are shown. Many interesting features appear in the two sections.

(1) The difference function is negative in the large square interstices, because ions are more contracted in the solid than when isolated, as a consequence of the Madelung field.

(2) For oxygen, the main feature is a charge transfer from the Mn–O–Mn axis to the orthogonal directions, as already commented on above; however, the bond region midway between Mn and O is excluded from this electron transfer and a small build-up of charge indicates some degree of covalent bonding. In the manganese core region there is a clear charge transfer from the $e_g$ to the $t_{2g}$ states (see the alternating positive and negative 'leaves' on the atom), which is particularly evident in the (110) section, to the right. A fraction of an electron is transferred to the external atomic region (see the flat square belt surrounding the atom).

(3) The right-hand figure shows that $Ca^{2+}$ has essentially the same charge distribution in the solid and in the isolated ion.

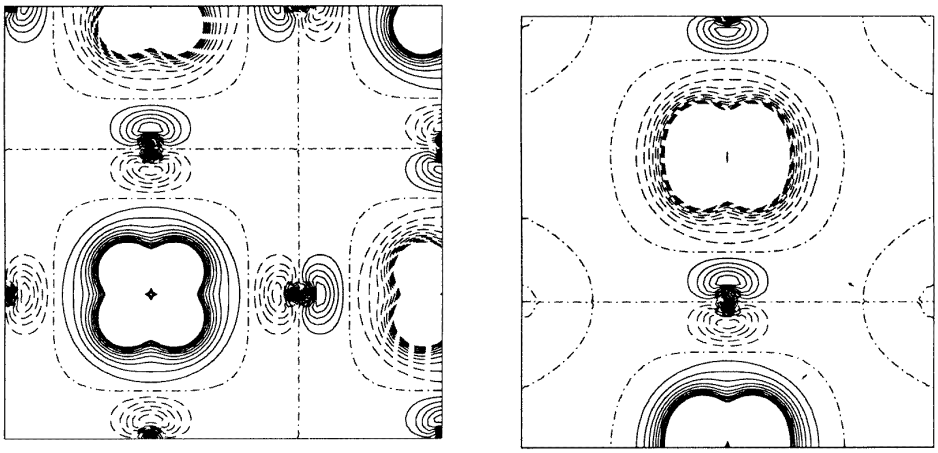

**Figure 5.** Spin-density maps ($\alpha$- minus $\beta$-electrons) for the antiferromagnetic solution. The separation between contiguous isodensity lines is 0.005 $e$ Bohr$^{-3}$; the function is truncated in the core region at $\pm 0.05$ $e$ Bohr$^{-3}$. The sections and symbols are as in figure 4.

Spin-density maps for the AFM and FM solutions are reported in figures 5 and 6, respectively. The three unpaired electrons are nearly totally localized on Mn; the spin density in the inner atomic part clearly shows the $t_{2g}$ shape, resulting from the filling of the $d_{xy}$ $d_{xz}$ and $d_{yz}$ orbitals; it is more spherical in the outer part, because of additional contributions from $e_g$ ($d_{x^2-y^2}$ and $d_{z^2}$) electrons. It is interesting to note that a non-negligible spin polarization appears on oxygen ($-0.06$ $|e|$; see the tables) in the FM solution whose origin and importance will be discussed in the next subsection.

### *3.3. The magnetic properties*

At the equilibrium geometry ($a = 3.75$ Å), the AFM state is more stable than the FM one by 0.066 eV. Under compression the energy difference between the two states, $\Delta E$, increases linearly (from 0.066 to 0.11 eV for $a = 3.75$ to 3.45 Å); this behaviour is very different from that shown by more ionic compounds, such as $KNiF_3$ and $KMnF_3$, where the increase of $\Delta E$ is exponential (see figure 2 in reference [3] and reference [2]). A similar exponential behaviour is shown also by NiO [9] and MnO [20], although the exponent coefficient is smaller than in the case of fluorides. In the present case minor charge displacements within the anion (see the discussion below concerning table 2) take place

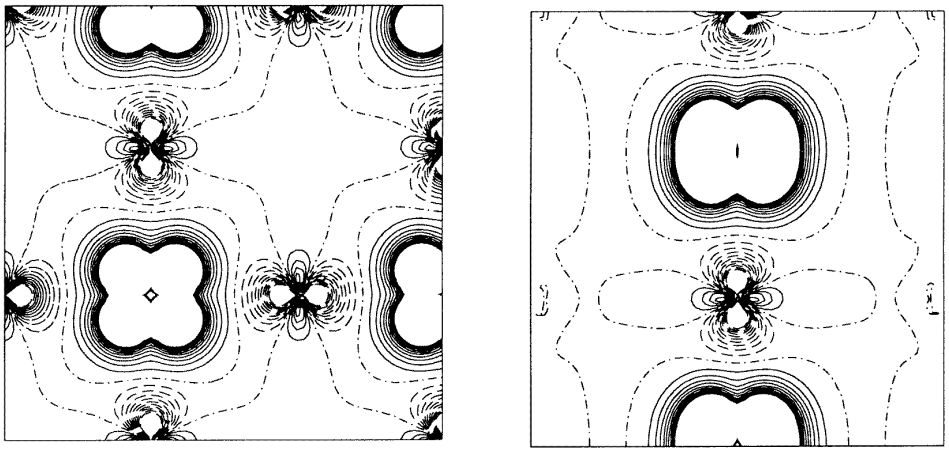

**Figure 6.** Spin-density maps for the ferromagnetic solution; the sections, symbols and scale are as in figure 5.

reducing the short-range repulsion between ions, which is responsible for the increasingly lower stability under compression of the FM with respect to the AFM phase. A similar rearrangement mechanism is energetically much more expensive in $KNiF_3$, where the ions are rigid closed-shell spherical balls [3].

The experimental [21, 22] superexchange magnetic constant $J$ quoted in Anderson's paper [23] can be related to $\Delta E$ through the following relation:

$$\Delta E = z|J|S^2 \tag{1}$$

if the Ising model Hamiltonian is assumed; in the above equation, $z$ is the number of Mn–Mn next-nearest neighbours and $S$ is the spin of the Mn ion ($S = 3.25/2$ in the present case; see table 1). The $J$-value calculated through equation (1) ($J_{calc} = -49$ K) turns out to be about five times larger than the experimental one ($J_{exp} = -9.2$ K). Apart from possible inaccuracies in the experimental determination, part of the discrepancy must be attributed to the differences between the geometry of the ideal cubic structure here adopted and the experimental orthorhombic structure: on the basis of general considerations [1, 2, 24] and of previous calculations [3, 19] the longer Mn–O distance and the non-linear superexchange Mn–O–Mn path are expected to reduce drastically the $J$-value obtained with the cubic symmetry.

Tables 1 and 2 show that the electron charge distributions are very similar for the FM and AFM phases; this is true also for the spin densities. Figures 5 and 6 are very similar with a small but very important difference: the spin polarization of the oxygen atom is higher in the FM case, as is easily seen by counting the number of isolines in figures 5 and 6. This difference is responsible for the higher stability of the AFM phase with respect to the FM phase. In fact, in a system where the bonding has large ionic components, the equilibrium geometry is determined by the balance between electrostatic attraction among the ions and short-range (exchange, or Pauli) repulsion between electrons belonging to first-nearest neighbours. As the Mn atom has more $\alpha$- than $\beta$-electrons (see table 1), mainly localized in $t_{2g}$ d states, oxygen $\alpha$-electrons feel a stronger repulsion from Mn electrons (due to the exclusion principle) and displace from the Mn–O–Mn region moving in orthogonal directions; this is reflected by the negative spin density in the bond region (dashed lines)

and the positive spin density in the orthogonal direction. Table 1 shows that Mulliken population analysis attributes a small negative ($-0.06$) electronic spin momentum to oxygen in the FM state resulting from $-0.013\ |e|$ in $p_x$ and $+0.003\ |e|$ in $p_y$ and $p_z$; the electron displacement of oxygen is then the way in which the system reduces short-range repulsion in the FM state. In the AFM case, a different mechanism is available for the reduction of Pauli repulsion: as the two Mn-atom first-nearest neighbours of oxygen have opposite spin, oxygen $\alpha$-electrons can move slightly towards the $\beta$-polarized Mn atom, and vice versa. This mechanism is energetically less expensive, and thus the AFM phase is more stable than the FM phase. Additional information on the difference between the FM and AFM phases can be obtained from figure 2. The FM PDOS are more diffuse than in the AFM case, because the interaction propagates into the crystal through the stronger Mn–O–Mn repulsion, generating higher dispersion in reciprocal space and hence less atom-like peaks in the DOS.

## 4. Conclusions

The *ab initio* quantum mechanical Hartree–Fock method has been shown to provide a consistent description of the structural electronic and magnetic properties of $CaMnO_3$ in its ideal cubic phase. A mechanism for explaining the greater stability of the antiferromagnetic phase with respect to the ferromagnetic one has been proposed. The present study represents a good starting point for further much more computationally demanding investigations, aimed at elucidating the effect of the rotation of the $MnO_6$ octahedra in going from the (ideal) cubic to the (experimental) orthorhombic phase, and the effect of the presence of regular oxygen vacancies on the electronic, magnetic and structural properties [6, 7]. Recent improvements in the CRYSTAL code and the rapid evolution in computer performance should soon permit us to tackle these problems.

## Acknowledgments

The work was supported by the Human Capital & Mobility Programme of the European Community under contract CHRX-CT93-0155; financial support from CSI Piemonte, from the Italian Ministero dell'Università e della Ricerca Scientifica e Tecnologica (MURST, 60%) and from the Italian CNR (Consiglio Nazionale delle Ricerche) is gratefully acknowledged.

## References

[1] de Jongh L J and Miedema A R 1974 *Adv. Phys.* **23** 1
[2] de Jongh L J and Block R 1975 *Physica* B **79** 568
[3] Ricart J M, Dovesi R, Roetti C and Saunders V R 1995 *Phys. Rev.* B **52** 2381
[4] Dovesi R, Ricart J M, Saunders V R and Orlando R 1995 *J. Phys.: Condens. Matter* **7** 7997
[5] Salje E K H 1990 *Phase Transitions in Ferroelastic and Co-elastic Crystals* (Cambridge: Cambridge University Press) p 283
[6] Poeppelmeier K R, Leonowicz M E, Scanlon J C and Longo J M 1982 *J. Solid State Chem.* **45** 71
[7] Leonowicz M E, Poeppelmeier K R and Longo J M 1985 *J. Solid State Chem.* **59** 71
[8] MacChesney J B, Williams H J, Potter J F and Sherwood R C 1967 *Phys. Rev.* B **164** 779
[9] Aprà E 1993 *PhD Thesis* Università di Torino
[10] Mackrodt W C, Harrison N M, Saunders V R, Allan N L, Towler M D, Aprà E and Dovesi R 1993 *Phil. Mag.* A **68** 653
[11] Towler M D, Allan N L, Harrison N M, Saunders V R, Mackrodt W C and Aprà E 1994 *Phys. Rev.* B **50** 5041

[12] Catti M, Valerio G and Dovesi R 1995 *Phys. Rev.* B **51** 7441
[13] Towler M D, Dovesi R and Saunders V R 1995 *Phys. Rev.* B **52** 10 150
[14] Dovesi R, Saunders V R and Roetti C 1992 *CRYSTAL92 User's Manual* Gruppo di Chimica Teorica, Università di Torino
[15] Pisani C, Dovesi R and Roetti C 1988 *Hartree–Fock ab initio Treatment of Crystalline Systems (Springer Lecture Notes in Chemistry 48)* (Heidelberg: Springer)
[16] Saunders V R, Freyria Fava C, Dovesi R, Salasco L and Roetti C 1992 *Mol. Phys.* **77** 629
[17] Catti M, Dovesi R, Pavese A and Saunders V R 1991 *J. Phys.: Condens. Matter* **3** 4151
[18] D'Arco P, Sandrone G, Dovesi R, Orlando R and Saunders V R 1993 *Phys. Chem. Minerals* **20** 407
[19] Freyria Fava F 1995 *Tesi di Laurea* Università di Torino
[20] Dovesi R and Freyria Fava F 1995 unpublished results
[21] Smart J S 1959 *Phys. Chem. Solids* **11** 97
[22] Wollan E O and Koehler W C 1955 *Phys. Rev.* **100** 545
[23] Anderson P W 1963 *Solid State Physics* vol 14 (New York: Academic) p 99
[24] Cox P A 1992 *Transition Metal Oxides* (Oxford: Clarendon)